JOURNAL OF SOLID STATE CHEMISTRY 115, 197–203 (1995)

Powder X-Ray and Neutron Diffraction Studies of the $(Ba_{1-x}Sr_x)_2(Sr_{0.67}Bi_{0.33})(Pb_{1-y}Bi_y)O_{6-\delta}$ Compounds with the $(NH_4)_3FeF_6$ Structure Type

C. Eylem and B. W. Eichhorn[1]

Center for Superconductivity Research and Department of Chemistry, University of Maryland, College Park, Maryland 20742

Q. Huang

Department of Materials and Nuclear Engineering, University of Maryland, College Park, Maryland, and National Institute of Standards and Technology, Gaithersburg, Maryland 20742

and

T. Clinton

Center for Superconductivity Research and Department of Physics, University of Maryland, College Park, Maryland 20742

Received February 28, 1994; in revised form June 13, 1994; accepted June 16, 1994

A new series of compounds of composition $(Ba_{1-x}Sr_x)_2(Sr_{0.67}Bi_{0.33})(Pb_{1-y}Bi_y)O_{6-\delta}$ has been prepared and characterized by powder X-ray and neutron diffraction studies. The phases adopt the cubic $(NH_4)_3FeF_6$ type structure (space group $Fm3m$) with Sr^{2+} ions occupying the B sites. TGA and neutron refinements show oxygen vacancies and a large anisotropy associated with the O atoms. The anisotropy is discussed in terms of a vacancy model.

INTRODUCTION

The bismuth and lead oxide Ruddlesden–Popper (R–P) phases of formula $Ba_{n+1}B_nO_{3n+1}$ where B = Pb, Bi represent a remarkable class of compounds with diverse structural and physical properties. For example, both bismuth and lead have $BaBO_3$ ($n = \infty$) perovskite-type end members but the structures of the two phases are quite different. $BaPbO_3$ adopts a simple cubic perovskite structure and becomes superconducting with partial Bi substitution (for $BaPb_{0.70}Bi_{0.30}O_3$, T_c = 13 K) (1, 2). In contrast, $BaBiO_3$ contains a 1 : 1 mixture of Bi^{3+} and Bi^{5+} ions ordered on different crystallographic sites in a slightly distorted cell with $I2/m$ symmetry (3, 4). Substituting alkali ions for Ba destroys the Bi^{3+}/Bi^{5+} ordering and induces superconductivity (for $Ba_{0.60}K_{0.40}BiO_3$, T_c = 30 K; for $Ba_{0.65}Rb_{0.35}BiO_3$, T_c = 29 K) (5, 6).

The lower n members of the $Ba_{n+1}Pb_nO_{3n+1}$ R–P phases are known for n = 1, 2, and 3 and have the prototypical $I4/mmm$ crystal symmetry (1, 7–9). Up to 50% Bi-for-Pb substitution can be obtained in these phases but, despite the existence of metal–insulator transitions in some of the series, superconductivity has not been observed (8–10). Recently, the first example of a two-dimensional superconductor in this class of compounds was identified in potassium- and bismuth-substituted phases of composition $Ba_{1.9}K_{0.1}Pb_{1-y}Bi_yO_4$ (n = 1, K_2NiF_4 structure). The y = 0.15 phase becomes superconducting at 14 K (11).

The lower n members of the pure $Ba_{n+1}Bi_nO_{3n+1}$ R–P phases are not known. However, potassium-for-barium substitution allows for the isolation of the $Ba_{1.7}K_{1.3}Bi_2O_7$ (n = 2) phase, which is also non-superconducting (12), but an n = 1 end member of any type has yet to be prepared. The phase of composition Ba_2BiO_4 is known but is part of a larger class of $Ba_{2+x}Bi_{2-x}O_{6-y}$ compounds that are not of the R–P type (13–17). Recent studies have shown that these phases adopt unusual $(NH_4)_3FeF_6$ type structures (1 : 1 ordered double-cubic perovskite) with Ba^{2+} distributed on both A and B sites of the lattice (15–17). The structure of the $Ba_2BiO_{4-\delta}$ phase is dependent upon synthesis conditions (16). For example, one can obtain 1 : 1 ordered ($(Ba_{5/3}Bi_{1/3})BaBiO_{5.67}$), 2 : 1 ordered ($Ba_3BaBi_2O_9$), or disordered ($Ba(Ba_{1/3}Bi_{2/3})O_3$) phases by modifying synthesis procedures (16). Neutron diffraction studies on different phases in the $Ba_{2+x}Bi_{2-x}O_{6-y}$ system revealed the prototypical cubic $(NH_4)_3FeF_6$ structure ($Fm3m$ symmetry) along with two lower symmetry phases of rhombohedral and monoclinic symmetries (17). Due to

[1] To whom correspondence should be addressed.

0022-4596/95 $6.00

the isolated nature of the BiO_6 octahedra in these compounds, they are neither metallic nor superconducting.

Because the layered K_2NiF_4 structure type is known to support metallic and superconducting behavior in the copper oxides as well as the K–Ba–Pb–Bi–O compounds, we became interested in studying the compositional ranges and properties of the K_2NiF_4-type Pb/Bi oxides at the edge of structural instability. In a previous paper (18), we reported that the $(Sr_{1-x}Ba_x)_2PbO_4$ phases adopt the K_2NiF_4 structure type when $0.5 \leq x \leq 1.0$. This isovalent substitution allows one to systematically compress the Pb–O distances up to the edge of instability of the K_2NiF_4 phase at $x = 0.5$ ($c/a \approx 3.0$). Slight changes in the in-plane M–O distances of the copper and vanadium R–P phases are known to have significant effects on the magnetic and transport properties (19, 20). Unfortunately, our attempts to substitute Bi-for-Pb in the $(Sr_{1-x}Ba_x)_2PbO_4$ compounds within a K_2NiF_4 framework were unsuccessful. However, during the course of our studies, we discovered an interesting new series of cubic $(NH_4)_3FeF_6$ type phases of general formula $(Ba_{1-x}Sr_x)_2(Sr_{0.67}Bi_{0.33})(Pb_{1-y}Bi_y)O_{6-\delta}$. In this paper, we describe the synthesis and structural characterization of these compounds and discuss their crystal chemistry with respect to the related $Ba_{2+x}Bi_{2-x}O_{6-y}$ (17) and $Sr_{10}Bi_6O_{24-\delta}$ (21) phases.

EXPERIMENTAL

Synthesis

The samples with the composition $(Ba_{1-x}Sr_x)_2Pb_{1-y}Bi_yO_{4-\delta}$ were prepared from stochiometric mixtures of $BaCO_3$ (99%), $SrCO_3$ (99.999%), Bi_2O_3 (99.9%), and PbO (99.9%). The reagents were intimately ground and pressed into pellets and placed into alumina boats. The samples were heated at a rate of 10°C/min in flowing O_2 at 600°C (1 day), 700°C (1 day), 800°C (1 day), and 900°C (1 day) with three intermediate grindings. The samples were then cooled to room temperature at a rate of 15°C/min. Annealing at 900°C did not cause any significant changes in X-ray diffraction profiles or cell constants.

Sr and Pb contents of selected samples were determined by an atomic absorption spectroscopy. Single phase compounds were dispersed in lithium borate fluxes ($LiBO_2$), dissolved in dilute HNO_3 (5%) and then analyzed using a Perkin–Elmer 2380 atomic absorption spectrometer. Sr and Pb contents were measured in duplicate and the average determination is listed in Table 1.

Oxygen contents were determined using a DuPont 951 thermogravimetric analyzer. The samples (~70 mg) were heated to 600°C at a rate of 10°C/min in flowing 10% H_2/Ar mixture (flow rate = 30 ml/min) and kept at 600°C until complete reduction to BaO, SrO, Pb, and Bi was accomplished. The final reduction products were characterized by X-ray diffraction. Each sample was analyzed twice with the average oxygen contents reported in Table 1.

Structural Characterization

The samples were routinely characterized by powder X-ray diffraction and selected samples were studied by neutron diffraction. X-ray diffraction data were collected at 25°C on a modified Phillips XRG 2000 diffractometer (Cu$K\alpha$ radiation) interfaced with a RADIX databox and MDI software system. Cell refinements were performed on all data collected between $20° < 2\theta < 70°$, and were corrected for sample displacement and zero-point error. The structures of $(Ba_{0.67}Sr_{0.33})_2(Sr_{0.67}Bi_{0.33})(Pb_{0.13}Bi_{0.87})O_{5.6}$ and $(Ba_{0.67}Sr_{0.33})_2(Sr_{0.67}Bi_{0.33})(Pb_{0.67}Bi_{0.33})O_{5.2}$ were determined from profile analyses of the X-ray and neutron powder diffraction data. Rietveld X-ray profile analyses (Micro-Riet, MDI) were performed on a Compuadd 386 personal computer. Data were collected at 0.02° intervals with 10 sec count rates. The data were indexed and refined in $Fm3m$ symmetry by using $(NH_4)_3FeF_6$ fractional coordinates as the initial structure model and Pearson VII profile shape functions. Due to the difficulty in distinguishing Pb and Bi by X rays, we have treated Pb atoms as Bi atoms. The occupancies of the various ions were fixed at values required by the compound stoichiometries. Rietveld refinements of the $(Ba_{0.67}Sr_{0.33})_2(Sr_{0.67}Bi_{0.33})(Pb_{0.13}Bi_{0.87})O_{5.6}$ and $(Ba_{0.67}Sr_{0.33})_2(Sr_{0.67}Bi_{0.33})(Pb_{0.67}Bi_{0.33})O_{5.2}$ yielded final residuals of $R_p = 8.0\%$, $R_{wp} = 10.4\%$, and $R_p = 8.3\%$, $R_{wp} = 11.9\%$, respectively.

Constant wavelength powder neutron diffraction intensity data for the $y = 0.33$ and 0.87 members of the $(Ba_{0.67}Sr_{0.33})_2(Sr_{0.67}Bi_{0.33})(Pb_{1-y}Bi_y)O_{6-\delta}$ phases were collected at room temperature using the 32 detector high resolution diffractometer located at the research reactor of the National Institute of Standards and Technology. The experimental conditions are summarized in Table 2. The structural refinements from the profile analysis of the neutron data were performed with the GSAS program of Larson and Von Dreele (22) using the intensity data in the 2θ range from 15° to 140° and $Fm3m$ crystal symmetry. The initial parameters for $(Ba_{0.67}Sr_{0.33})_2(Sr_{0.67}Bi_{0.33})(Pb_{1-y}Bi_y)O_{6-\delta}$ structural refinements were taken from the X-ray studies. Various models were employed that contained Sr, Bi, and Pb distributed over various lattice sites. The best fits were obtained from models with $(Sr_{0.67}Bi_{0.33})$ B-site and $(Pb_{1-y}Bi_y)$ B'-site occupancies, with oxygen vacancies and anisotropic thermal parameters. The background in the neutron diffraction profiles was not modeled because of the large signal to noise ratio. The neutron diffraction profiles shown in Figs. 3 and 4 contain small backgrounds in the range of 30°–40° which might be a sign of diffuse scattering due to short-range ordering. A summary of the final residuals from the various models is given in Table 3.

TABLE 1
Atomic Absorption and Thermogravimetric Analyses of the $(Ba_{1-x}Sr_x)_2(Sr_{0.67}Bi_{0.33})(Pb_{1-y}Bi_y)O_{6-\delta}$ Compounds

System	%Sr[a]	%Pb[a]	Oxygen content		
			Observed[b]	Calculated[c]	Neutron[d]
$x = 0.33$; $y = 0.87$	—	—	5.6	5.59	5.77
$x = 0.33$; $y = 0.73$	19(18)	5(8)	—	5.52	—
$x = 0.33$; $y = 0.33$	18(18)	18(21)	5.2	5.32	5.17
$x = 0.60$; $y = 0.33$	26(25)	16(22)	5.2	5.32	—

[a] Weight percent determined by atomic absorption spectroscopy. Theoretical percentages are given in parenthesis.
[b] Oxygen contents determined by thermogravimetric analysis.
[c] Oxygen contents calculated based on the general formula $(Ba_{1-x}Sr_x)_2(Sr_{0.67}Bi^{3+}_{0.33})(Pb^{4+}_{1-y}Bi^{5+}_y)O_{6-\delta}$.
[d] Oxygen contents obtained from profile refinements of neutron diffraction data.

RESULTS AND DISCUSSION

A general survey of the Sr_2PbO_4–Ba_2PbO_4–Sr_2BiO_4–Ba_2BiO_4 phase field (Fig. 1) shows three principle structure types; namely the K_2NiF_4 (KNF), $(NH_4)_3FeF_6$ (NFF), and Sr_2PbO_4 (SPO) types. We previously observed that the $(Sr_{1-x}Ba_x)_2PbO_4$ solid solutions form biphasic SPO + KNF mixtures for $0 \leq x \leq 0.5$ and single phase KNF compounds for $0.5 \leq x \leq 1.0$ (18). The $Ba_2(Pb_{1-x}Bi_x)O_4$ solid solution was previously studied by Xu *et al.* (10) and shown to maintain the KNF structure for $0 \leq x \leq 0.30$. The Ba_2BiO_4 phase possesses an NFF structure however its solid solution chemistry with Sr or Pb has not been reported. Sr_2BiO_4 phase is not known but Sr-rich $Sr_2Bi_{1-x}Sr_xO_4$ compounds (not represented in Fig. 1) with the NFF type structure have been reported (21). In the present study, we have found that Bi-for-Pb substitutions in the $(Sr_{1-x}Ba_x)_2PbO_4$ phases result in single phase cubic NFF compounds in certain regions of the phase diagram (shaded region in Fig. 1). These compounds can be described using the conventional NFF $A_2BB'O_{6-\delta}$ nomenclature system, by the general formula $(Ba_{1-x}Sr_x)_2(Sr_{0.67}Bi_{0.33})(Pb_{1-y}Bi_y)O_{6-\delta}$ where $\sim 0.9 \leq x \leq \sim 0.45$, $0.33 \leq y \leq 0.87$, and $0.8 \leq \delta \leq 0.4$. The remainder of the compositions inside the dotted lines in Fig. 1 are biphasic comprising mixtures of NFF and KNF compounds. The compositions outside the dotted lines were not investigated.

In order to investigate the nature of the cation ordering and structural distortions, Rietveld analyses were conducted on the X-ray and neutron diffraction profiles of the $y = 0.87$ and 0.33 members of the $(Ba_{0.67}Sr_{0.33})_2(Sr_{0.67}Bi_{0.33})(Pb_{1-y}Bi_y)O_{6-\delta}$ series. These refinements, together with the TGA and atomic absorption analyses, showed oxygen anisotropy, disordered oxygen vacancies, Sr^{2+} ions on the NFF *A* and *B* sites and segregation of Bi^{3+} and Bi^{5+} ions on the NFF *B* and *B'* sites, respectively. These results are described individually below.

The X-ray profiles of the $(Ba_{1-x}Sr_x)_2(Sr_{0.67}Bi_{0.33})(Pb_{1-y}Bi_y)O_{6-\delta}$ compounds were indexed on face-centered cubic lattices with $a \approx 8.6$ Å (see Fig. 2). Rietveld profile analy-

TABLE 2
Experimental Conditions for Powder Neutron Diffraction Data Collection

Monochromatic beam	311 reflection of Cu monochromator
Wavelength	1.540(1) Å
Horizontal divergences	15', 20', 7' of arc for the in-pile, monochromatic beam, and diffracted beam collimators, respectively
Sample container	Vanadium can
2θ Angular range	4°–164°; steps: 0.05°
Scattering amplitudes (10^{-12} cm)	b(Sr) = 0.702, b(Ba) = 0.525, b(Pb) = 0.940, b(Bi) = 0.853, b(O) = 0.581
Temperature	296 K

TABLE 3
Agreement Factors[a] for Various Structural Models (Neutron Diffraction) for the $(Ba_{0.67}Sr_{0.33})_2(Sr_{0.67}Bi_{0.33})(Pb_{1-y}Bi_y)O_{6-\delta}$ Compounds

	$y = 0.87$			$y = 0.33$		
	R_p (%)	R_{wp} (%)	χ^2	R_p (%)	R_{wp} (%)	χ^2
Isotropic	8.88	12.29	3.047	8.06	10.49	2.715
Oxygen anisotropic	7.34	9.65	1.877	7.17	8.61	1.830
Oxygen occupancy varied	7.23	9.59	1.865	6.58	7.97	1.568

[a] R_p (profile factor) = $\{[\sum_i (I_i^{obs} - I_i^{calc})^2]\}^{1/2}$; R_{wp} = (weighted profile factor) = $\{[\sum_i w_i(I_i^{obs} - I_i^{calc})^2]/[\sum w_i(I_i^{obs})^2]\}^{1/2}$; and $\chi^2 = N_o - N_v / \sum[wI_o^2]$.

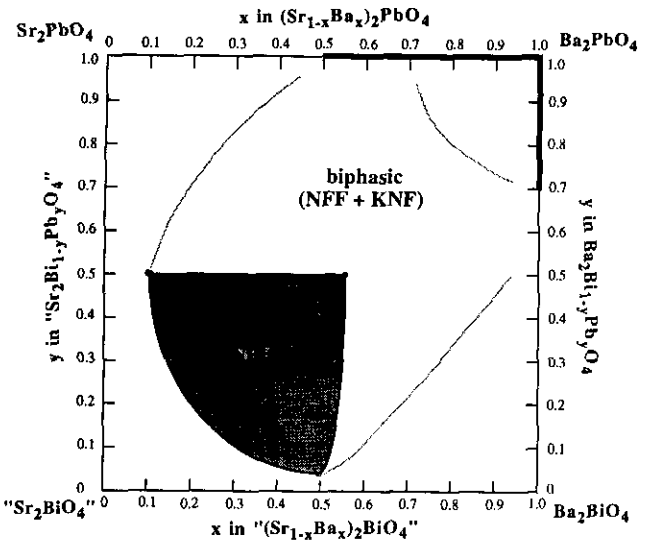

FIG. 1. Approximate structural phase field of the Sr_2PbO_4–Ba_2PbO_4–Sr_2BiO_4–Ba_2BiO_4 system. Single-phase KNF materials are represented by the heavy lines.

sis of the X-ray data for the $y = 0.87$ and 0.33 $(Ba_{0.67}Sr_{0.33})_2(Sr_{0.67}Bi_{0.33})(Pb_{1-y}Bi_y)O_{6-\delta}$ phases were conducted using the prototypical $Fm3m$ symmetry of the cubic NFF compounds. The most reasonable fits were obtained with 67% Sr/33% Bi and 100% Bi (or Pb) occupying NFF B and B' sites, respectively. The inability to distinguish Bi from Pb and problems associated with determining oxygen positions by X-ray diffraction greatly limited the amount of structural information attainable from these analyses.

To circumvent these problems, neutron diffraction experiments were performed on the $y = 0.87$ and 0.33 phases as well. The observed and calculated diffraction profiles

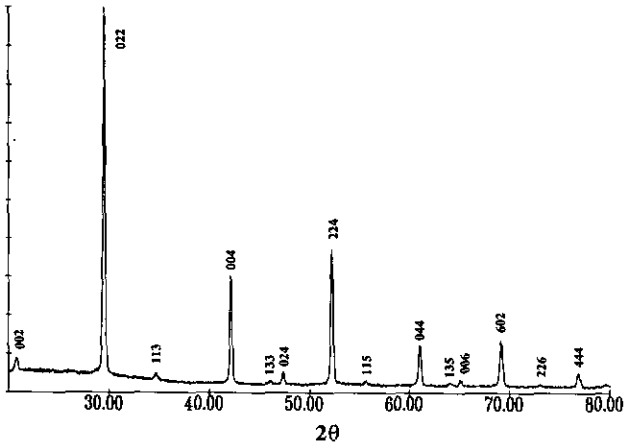

FIG. 2. Powder X-ray diffraction profile of the $(Ba_{0.67}Sr_{0.33})_2(Sr_{0.67}Bi_{0.33})(Pb_{0.13}Bi_{0.87})O_{5.6}$ sample.

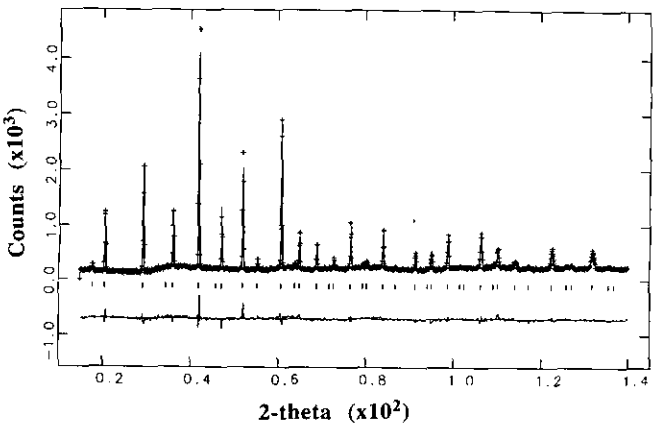

FIG. 3. Calculated (continuous line) and observed (crosses) neutron diffraction profile of $(Ba_{0.67}Sr_{0.33})_2(Sr_{0.67}Bi_{0.33})(Pb_{0.13}Bi_{0.87})O_{5.6}$. A difference curve ($I_{obs} - I_{calc}$) is plotted at the bottom (same scale).

are shown in Figs. 3 and 4 and the structural parameters are given in Tables 4 and 5. There was no evidence of orthorhombic, monoclinic, or tetragonal distortions similar to those observed in the related $Ba_{2+x}Bi_{2-x}O_{6-y}$ (17) and $Sr_{10}Bi_6O_{24-\delta}$ (21) phases. In addition, models with Ba on the B (or B') sites or Bi on the A sites yielded significantly poorer fits in contrast to the related $Ba_{2+x}Bi_{2-x}O_{6-y}$ phases (17). Like the X-ray refinements, the best results were obtained with a 67% Sr occupation on the NFF B-site. Because of the different scattering lengths of Bi and Pb, the neutron experiments allow for occupancy refinement of these elements on the B and B' lattice sites. The best fits were obtained with a fixed 67% Sr/33% Bi B-site population and a $Pb_{1-y}Bi_y$ population on the B' site. In addition, the highest quality profile fits were obtained by including oxygen vacancies. The refined oxygen contents for the $y = 0.87$ and 0.33 phases were 5.77 and 5.17,

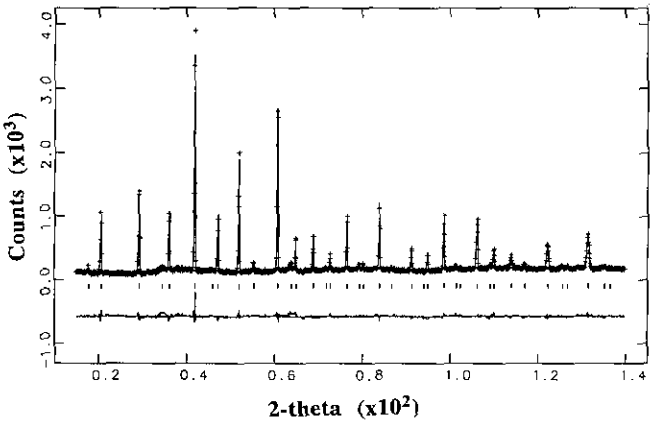

FIG. 4. Calculated (continuous line) and observed (crosses) neutron diffraction profile of $(Ba_{0.67}Sr_{0.33})_2(Sr_{0.67}Bi_{0.33})(Pb_{0.67}Bi_{0.33})O_{5.2}$. A difference curve ($I_{obs} - I_{calc}$) is plotted at the bottom (same scale).

TABLE 4
Refined Structural Parameters[a] for
$(Ba_{0.67}Sr_{0.33})_2(Sr_{0.67}Bi_{0.33})(Pb_{0.13}Bi_{0.87})O_{5.6}$

Atom	Site	x	y	z	Occupancy	B (Å^2)
Ba1	8*c*	0.25	0.25	0.25	0.667	2.52(5)
Sr1	8*c*	0.25	0.25	0.25	0.333	2.52(5)
Sr2	4*b*	0.5	0.5	0.5	0.667	2.1(1)
Bi1	4*b*	0.5	0.5	0.5	0.333	2.1(1)
Bi2	4*a*	0	0	0	0.867	0.64(6)
Pb1	4*a*	0	0	0	0.133	0.64(6)
O	24*e*	0.2386(5)	0	0	0.961(7)	
		B_{11} (Å^2)	B_{22} (Å^2)	B_{33} (Å^2)		
O		1.01(1)	8.9(1)	8.9(1)		

[a] Neutron diffraction, unit cell constant = 8.6177(1) Å.

respectively. These values are in reasonable agreement with the oxygen contents of 5.6 and 5.2 determined by TGA studies.

To accommodate the differences in average ionic radii at the *B* and *B'* sites, the oxygen is shifted from an idealized symmetrically bridging position (1/4, 0, 0) to a position closer to *B'* (~0.24, 0 0). This shift generates large BO_6 octahedra ($d_{B-O} \approx 2.24$ Å) centered at 1/2, 1/2, 1/2 and smaller $B'O_6$ octahedra ($d_{B-O} \approx 2.06$ Å) centered at the origin (see Fig. 5 and Table 6). Assuming that Bi^{3+} and Bi^{5+} order on different sites in the NFF structure, the most reasonable model would contain the large Bi^{3+} ion on the *B* site with Sr^{2+} and the smaller Bi^{5+} ion on the *B'* site with Pb^{4+}. The proposed $(Ba_{1-x}Sr_x)_2(Sr_{0.67}Bi^{3+}_{0.33})(Pb^{4+}_{1-y}Bi^{5+}_y)O_{6-\delta}$ formulations are consistent with the oxygen contents determined from the TGA data, the refined occupancies from the neutron studies (see Table 1), and the variations in structure resulting from Pb^{4+}-for-Bi^{5+} substitution on the *B'* site (discussed below). These findings are also consistent with the proposals of Chaillout *et al.* (23) that oxygen nonstoichiometry triggers Bi^{3+}/Bi^{5+} ordering on different crystallographic sites.

TABLE 5
Refined Structural Parameters[a] for
$(Ba_{0.67}Sr_{0.33})_2(Sr_{0.67}Bi_{0.33})(Pb_{0.67}Bi_{0.33})O_{5.2}$

Atom	Site	x	y	z	Occupancy	B (Å^2)
Ba1	8*c*	0.25	0.25	0.25	0.667	3.66(6)
Sr1	8*c*	0.25	0.25	0.25	0.333	3.66(6)
Sr2	4*b*	0.5	0.5	0.5	0.667	2.5(1)
Bi1	4*b*	0.5	0.5	0.5	0.333	2.5(1)
Bi2	4*a*	0	0	0	0.333	1.21(8)
Pb1	4*a*	0	0	0	0.667	1.21(8)
O	24*e*	0.2403(6)	0	0	0.861(6)	
		B_{11} (Å^2)	B_{22} (Å^2)	B_{33} (Å^2)		
O		0.8(1)	7.6(1)	7.6(1)		

[a] Neutron diffraction, unit cell constant = 8.6039(2) Å.

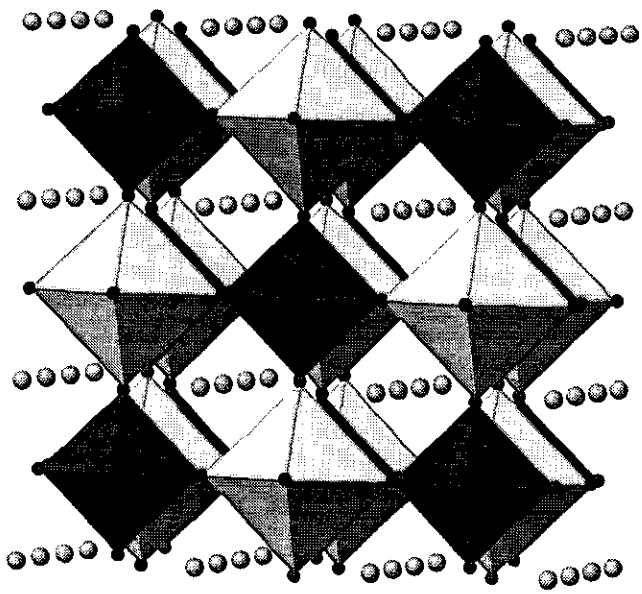

FIG. 5. Polyhedral representation of the structure of $(Ba_{0.67}Sr_{0.33})_2(Sr_{0.67}Bi_{0.33})(Pb_{0.67}Bi_{0.33})O_{5.2}$. The dark and light octahedra represent $(Pb,Bi)O_6$ and $(Sr,Bi)O_6$, respectively. The light spheres represent the *A* site $(Ba_{0.67}Sr_{0.33})$ ions and dark spheres represent oxygens.

The variations in cell parameters as a function of *x* and *y* of the $(Ba_{1-x}Sr_x)_2(Sr_{0.67}Bi_{0.33})(Pb_{1-y}Bi_y)O_{6-\delta}$ system are shown in Fig. 6. The substitution of Sr-for-Ba decreases the unit cell constant as expected (Fig. 6a), however, the cell constant *increases* by ~0.2% when Pb^{4+} ($r = 0.915$ Å) (24) is replaced by the smaller Bi^{5+} ($r = 0.90$ Å) (24) (Fig. 6b). The neutron structural refinements of the two $(Ba_{0.67}Sr_{0.33})_2(Sr_{0.67}Bi_{0.33})(Pb_{1-y}Bi_y)O_{6-\delta}$ phases show that the $(Pb_{1-y}Bi_y)$–O distances decrease with increasing *y* as expected from Bi^{5+}-for-Pb^{4+} substitution. However, $(Ba_{0.67}Sr_{0.33})$–O and $(Sr_{0.67}Bi_{0.33})$–O distances increase with *y* and collectively affect the slight increase in the cell parameter. Presumably, the increase in coordination number due to fewer oxygen vacancies gives rise to larger *A*–O and *B*–O separations.

TABLE 6
Average Bond Lengths (Å) in the $(Ba_{0.67}Sr_{0.33})_2(Sr_{0.67}Bi_{0.33})(Pb_{1-y}Bi_y)O_{6-\delta}$ System

Bond	$y = 0.33$	$y = 0.87$
(Ba1/Sr1)–O	3.0431(2)	3.0484(1)
(Sr2/Bi1)–O	2.235(5)	2.253(4)
(Bi2/Pb1)–O	2.067(5)	2.056(4)

[a] Determined from neutron refinements.

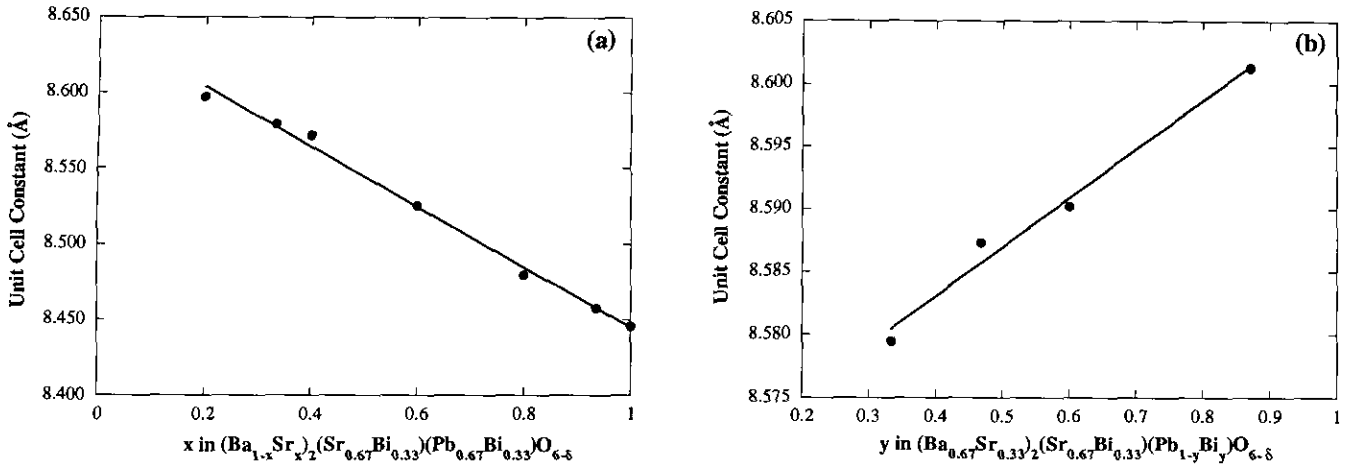

FIG. 6. (a) A plot of unit cell constants versus of x in the $(Ba_{1-x}Sr_x)_2(Sr_{0.67}Bi_{0.33})(Pb_{0.67}Bi_{0.33})O_{6-\delta}$ system. (b) A plot of unit cell constants versus y in the $(Ba_{0.67}Sr_{0.33})_2(Sr_{0.67}Bi_{0.33})(Pb_{1-y}Bi_y)O_{6-\delta}$ system.

The oxygen atoms in the two $(Ba_{0.67}Sr_{0.33})_2(Sr_{0.67}Bi_{0.33})(Pb_{1-y}Bi_y)O_{6-\delta}$ phases are highly anisotropic. An ORTEP drawing of the $B'O_6$ octahedron of the $(Ba_{0.67}Sr_{0.33})_2(Sr_{0.67}Bi_{0.33})(Pb_{0.67}Bi_{0.33})O_{5.2}$ phase is shown in Fig. 7 and the anisotropic thermal parameters for the two phases studied are given in Tables 4 and 5. Because of the different ions randomly distributed over the B and B' sites, one would anticipate a large anisotropy along the B–O–B' vector due to a static disorder of the O position. Instead, the anisotropies normal to the B–O–B' vector (B_{22} and B_{33}) are approximately eight times larger than along the B–O–B' vector (B_{11}) in the present compounds. The origin of these anisotropies most likely results from static distortions due to oxygen vacancies (17). The oxygen nonstoichiometries generate local MO_5 square pyramids in which the basal oxygens distort towards the missing sixth vertex (see Fig. 8). This static disorder is consistent with the observed thermal parameters.

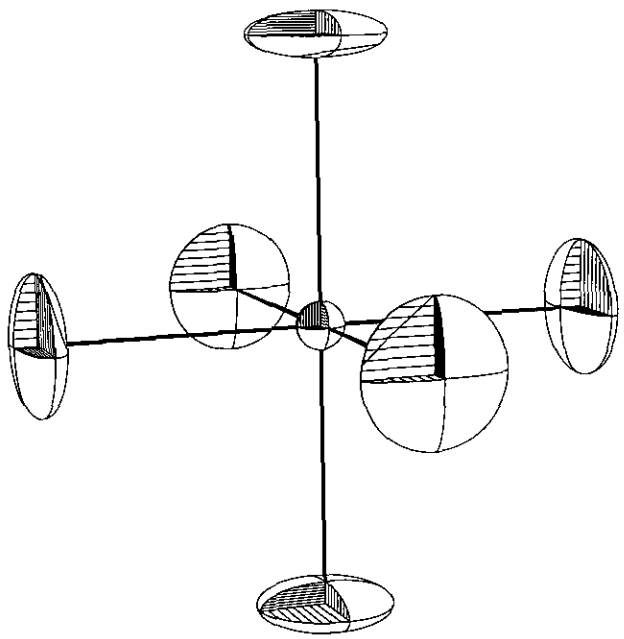

FIG. 7. ORTEP representation of the $(Sr_{0.67}Bi_{0.33})O_6$ octahedron in $(Ba_{0.67}Sr_{0.33})_2(Sr_{0.67}Bi_{0.33})(Pb_{0.67}Bi_{0.33})O_{5.2}$ showing the oxygen anisotropy.

The NFF compounds described above as well as the $Ba_{2+x}Bi_{2-x}O_{6-y}$ (17) and $Sr_{10}Bi_6O_{24-\delta}$ (21) phases contain alkaline earth ions on perovskite B sites and oxygen nonstoichiometries. The oxygen vacancies require the formation of BO_5 square pyramids comprising five-coordinate alkaline earth ions. It is plausible that oxygen vacancies are always associated with the Bi^{3+} ions on the B sites and Bi^{3+}–O_{vac} disorder in a pairwise fashion. However, if the vacancies are associated in disordered pairs, there must still be alkaline earth ions in square-pyramidal sites in compounds with large vacancy concentrations. This is especially surprising for the $Ba_{2+x}Bi_{2-x}O_{6-y}$ system (17) since the five-coordinate Ba^{2+} ion is not common. In our $(Ba_{1-x}Sr_x)_2(Sr_{0.67}Bi_{0.33})(Pb_{1-y}Bi_y)O_{6-\delta}$ phases, only Sr^{2+} migrates to the B-sites and five coordinate Ba^{2+} is avoided. The present compounds are of course closely related to the $Sr_{10}Bi_6O_{24-\delta}$ phase of general composition $Sr_2(Sr_{0.5}Bi^{3+}_{0.25}Bi^{5+}_{0.25})Bi^{5+}O_{6-\delta}$ (21), however, the distribution of Bi^{3+} and Bi^{5+} appears to be quite different.

Attempts to chemically substitute Ba^{2+} or Sr^{2+} by K^+ resulted in multiphase mixtures. Magnetic screening of these samples did not show any sign of superconductivity. Similar attempts to substitute potassium-for-barium in the related $Ba_2(Ba,Bi)O_6$ compounds were also not successful (15).

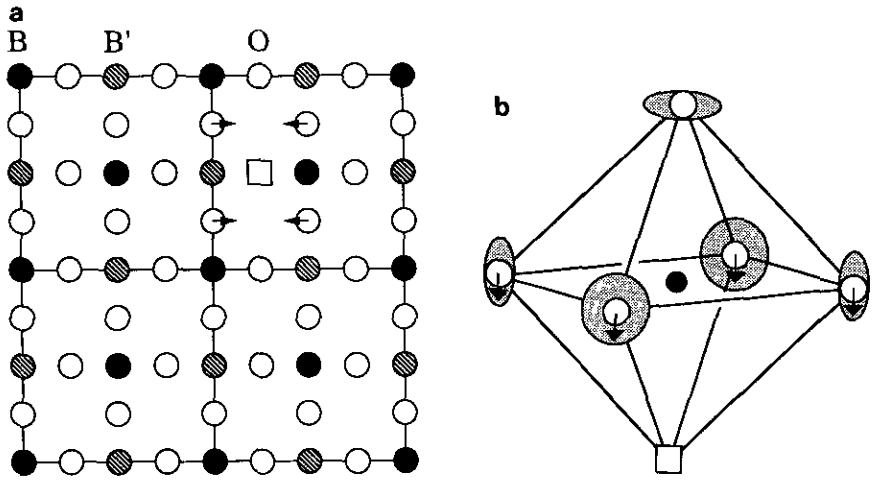

FIG. 8. The structural model proposed for oxygen anisotropy in the $(Ba_{1-x}Sr_x)_2(Sr_{0.67}Bi_{0.33})(Pb_{1-y}Bi_y)O_{6-\delta}$ phases. (a) Two-dimensional representation BO_6 and $B'O_6$ array. The square represents an oxygen vacancy. (b) Representation of oxygen shift and fivefold coordination due to an oxygen vacancy.

ACKNOWLEDGMENTS

We acknowledge the NSF (DMR-9223060) for financial support of this work. We thank Mr. H. L. Ju for assistance with the magnetic screening experiments.

REFERENCES

1. G. Wagner and H. Binder, *Z. Anorg. Allg. Chem.* **298,** 12 (1959).
2. A. W. Sleight, J. L. Gillson, and P. E. Bierstedt, *Solid State Commun.* **17,** 27 (1975).
3. D. E. Cox and A. W. Sleight, *Solid State Commun.* **19,** 969 (1976).
4. G. Thornton and A. J. Jacobson, *Acta Crystallogr. Sect. B* **34,** 351 (1978).
5. L. F. Mattheiss, E. M. Gyorgy, and D. W. J. Johnson, *Phys. Rev. B* **37,** 3745 (1988).
6. R. J. Cava, B. Batlogg, J. J. Krajewski, R. Farrow, L. W. Rupp, Jr., A. E. White, K. Short, W. F. Peck, and T. Kometani, *Nature* **332,** 814 (1988).
7. (a) R. Weiss and R. Faivre, *C.R. Acad. Sci.* **248,** 106 (1959); (b) H. Stoll and R. Hoppe, *Z. Anorg. Allg. Chem.* **548,** 165 (1987).
8. W. T. Fu, H. W. Zandergen, Q. Xu, J. M. Van Ruitenbeek, L. J. De Jongh, and G. Van Tendeloo, *Solid State Commun.* **70,** 1117 (1989).
9. R. J. Cava, H. Takagi, H. W. Zandbergen, B. Hessen, J. J. Krajewski, and W. F. Peck, *Phys. Rev. B* **46,** 14101 (1992).
10. Q. Xu, W. T. Fu, J. M. Ruitenbeek, and L. J. De Jongh, *Physica C* **167,** 271 (1990).
11. M. Licheron and F. Gervais, *J. Alloys Compounds* **195,** 77 (1993).
12. R. J. Cava, T. Siegrist, W. F. Peck, J. J. Krajewski, B. Batlogg, and J. Rosamilia, *Phys. Rev. B* **44,** 9746 (1991).
13. K. Kourtakis and M. Robbins, *Mater. Res. Bull.* **24,** 1287 (1989).
14. M. Itoh, T. Sawada, R. Liang, H. Kawaji, and T. Nakamura, *J. Solid State Chem.* **87,** 245 (1990).
15. M. Licheron, F. Gervais, J. Coutures, and J. Choisnet, *Solid State Commun.* **75,** 759 (1990).
16. K. P. Reis, A. J. Jacobson, and J. Kulik, *Chem. Mater.* **5,** 1070 (1993).
17. K. P. Reis, A. J. Jacobson, and J. M. Nicol, *J. Solid State Chem.* **107,** 428 (1993).
18. B.-H. Chen and B. W. Eichhorn, *J. Solid State Chem.* **97,** 340 (1992).
19. J. G. Bednorz and K. A. Muller, *Z. Phys. B* **64,** 189 (1986).
20. W. Gong, J. S. Xue, and J. E. Greedan, *J. Solid State Chem.* **91,** 180 (1991).
21. Bokhimi and M. Portilla, *J. Solid State Chem.* **105,** 371 (1993).
22. A. C. Larson and R. B. Von Dreele, General Structure Analysis System, University of California, 1985.
23. C. Chaillout, J. P. Remeika, A. Santoro, and M. Marezio, *Solid State Commun.* **56,** 829 (1985).
24. R. D. Shannon, *Acta Crystallogr. Sect. A* **32,** 751 (1976).